# The Architecture of Actin Filaments and the Ultrastructural Location of Actin-binding Protein in the Periphery of Lung Macrophages

John H. Hartwig and Patty Shevlin

Hematology-Oncology Unit, Massachusetts General Hospital, Department of Medicine, Harvard Medical School, Boston, Massachusetts 02114

*Abstract.* A highly branched filament network is the principal structure in the periphery of detergent-extracted cytoskeletons of macrophages that have been spread on a surface and either freeze or critical point dried, and then rotary shadowed with platinum-carbon. This array of filaments completely fills lamellae extended from the cell and bifurcates to form 0.2–0.5 μm thick layers on the top and bottom of the cell body. Reaction of the macrophage cytoskeletons with anti-actin IgG and with anti-IgG bound to colloidal gold produces dense staining of these filaments, and incubation with myosin subfragment 1 uniformly decorates these filaments, identifying them as actin. 45% of the total cellular actin and ~70% of actin-binding protein remains in the detergent-insoluble cell residue. The soluble actin is not filamentous as determined by sedimentation analysis, the DNAase I inhibition assay, and electron microscopy, indicating that the cytoskeleton is not fragmented by detergent extraction. The spacing between the ramifications of the actin network is 94 ± 47 nm and 118 ± 72 nm in cytoskeletons prepared for electron microscopy by freeze drying and critical point drying, respectively. Free filament ends are rare, except for a few which project upward from the body of the network or which extend down to the substrate. Filaments of the network intersect predominantly at right angles to form either T-shaped and X-shaped overlaps having striking perpendicularity or else Y-shaped intersections composed of filaments intersecting at 120–130° angles. The actin filament concentration in the lamellae is high, with an average value of 12.5 mg/ml. The concentration was much more uniform in freeze-dried preparations than in critical point-dried specimens, indicating that there is less collapse associated with the freezing technique.

The orthogonal actin network of the macrophage cortical cytoplasm resembles actin gels made with actin-binding protein. Reaction of cell cytoskeletons and of an actin gel made with actin-binding protein with anti-actin-binding protein IgG and anti-IgG-coated gold beads resulted in the deposition of clusters of gold at points where filaments intersect and at the ends of filaments that may have been in contact with the membrane before its removal with detergent. In the actin gel made with actin-binding protein, 75% of actin–fiber intersections labeled, and the filament spacing between intersections is consistent with that predicted on theoretical grounds if each added actin-binding protein molecule cross-links two filaments to form an intersection in the gel. On the other hand, only 38% of all filament intersections in the macrophage cortical cytoskeletons labeled, and the filament spacing between junctions is much smaller than that predicted from the molar ratio of actin-binding protein to actin in the cytoskeletons. Despite the differences between actin gels made with actin-binding protein and macrophage cytoskeletons, which presumably arise from the greater complexity of the cell compared with the purified protein assembly, the networks were qualitatively similar.

For over 200 years microscopists have recognized the particle-excluding nature of peripheral cytoplasm in ameboid cells (40). The appearance of this region, sometimes called hyaline ectoplasm or hyaloplasm, has long been ascribed to the existence of some kind of gel which excludes organelles and manifests elastic or contractile properties (24). It is now evident that actin filaments are principal structures in the peripheral cytoplasm, and that many actin-modulating proteins affect the assembly and interaction of actin polymers in vitro, including some proteins that promote the apparent gelation of actin (reviewed in reference 38). Therefore, it is possible that peripheral cytoplasm represents an actin filament gel.

Macrophages extend hyaline veils during spreading, locomotion, and phagocytosis (26), and this peripheral cytoplasm contains actin and several actin-associated proteins (1, 2, 4,

9, 36, 41). We have proposed that a high $M_r$ protein called actin-binding protein has an important role in the gelation of peripheral cytoplasm. The proposal is based on the evidence that actin-binding protein is very effective in producing an apparent sol-to-gel transformation of purified actin filaments in vitro (7, 19, 37) in contrast to α-actinin, the only other actin cross-linking protein isolated thus far from macrophages (3).

Actin filaments assembled in the presence of actin-binding protein display a distinctive morphology as determined by electron microscopy, being composed of perpendicular branching filaments (20, 30). Therefore, if a similar configuration of actin filaments can be observed in cortical cytoplasm, it is reasonable to conclude that actin-binding protein is responsible for it.

In this paper we provide quantitative morphometric data concerning the concentration and spacing of actin filaments in the periphery of rabbit lung macrophages treated with detergent. We report that short actin filaments predominate in the cortical lamellae of these cytoskeletons and intersect in three-dimensional space at high angles averaging either near 90° or 120–130°. This architecture is qualitatively similar to that of an actin gel made with actin-binding protein. In addition, we also localized the actin-binding protein molecules by immunoelectron microscopy and documented that the actin-binding protein label resides selectively at many points where filaments overlap in both macrophage cytoskeletons and in an actin gel made with actin-binding protein.

## Materials and Methods

### Macrophages

Macrophages were washed out of the lungs of New Zealand white rabbits by the method of Myrvik et al. (29). To increase cell yields, rabbits were given single intravenous injections of 1 ml of complete Freund's adjuvant (Cappel Laboratories, Cochranville, PA) containing 5 mg of lyophilized Bacillus Calmette-Guerin (University of Illinois at Chicago, Health Sciences Center, Chicago, IL) 2–3 wk before pulmonary lavage. The lung macrophages were washed twice by centrifugation at 280 *g* in 0.15 M NaCl and then suspended in 98 vol of Krebs–Ringer Phosphate buffer, pH 7.4 (KRP) without added $CaCl_2$. The animals used in this study were maintained in accordance with guidelines of the National Research Council.

### Attachment of Cells for Microscopy

200 mesh nickel grids (Ted Pella, Inc., Tustin, CA) were coated with a 0.3% formvar film and picked up on the glass coverslips. Drops of a 2% macrophage suspension in KRP were placed on grids attached to glass coverslips 5 mm in diameter or to formvar-coated coverslips without grids and incubated at room temperature for 3 min. The formvar-coated surfaces were subjected to glow discharging in a JEE-4X evaporator for 2 min just before application of macrophages. The coverslips containing cells were then rinsed with KRP to remove non-adherent cells, covered with KRP solution containing 1% fresh rabbit serum, and warmed to 37°C in a humidified atmosphere for 10 to 15 min.

### Preparation of Cytoskeletons for Electron Microscopy

The procedure used was an adaptation of the detergent extraction method of Schliwa and van Blerkom (33, 34). All of the following steps were carried out at 37°C. Before detergent extraction, the cells were rinsed briefly in 60 mM Pipes, 25 mM Hepes, 10 mM EGTA, and 2 mM $MgCl_2$, pH 6.9 (PHEM buffer of Schliwa and van Blerkom [33]) and then dipped in PHEM buffer containing 0.75% Triton X-100 for 2 min. The detergent-permeabilized cells (cytoskeletons) were washed briefly in PHEM and then fixed for 10 min in 10 mM sodium phosphate buffer containing 1% glutaraldehyde–0.2% tannic acid, pH 7.0. After fixation, salt was removed from the specimens by washing the cytoskeletons in distilled water. Cytoskeletons to be critical point dried were then stepwise dehydrated with increasing concentrations of ethanol and critical point dried from bone-dry $CO_2$ in an Autosamdri 810 critical point dryer (Tousimis Research Corp., Rockville, MD) equipped with a water trapping filter. Coverslips containing cytoskeletons to be freeze dried were placed in 15% methanol, mounted on the stage of plunger arm of the rapid freezing device (Med-Vac, Inc., St. Louis, MO), blotted with filter paper, and then frozen on a liquid helium–cooled copper block as described by Heuser and Kirschner (22). Frozen specimens were freeze dried in a Balzers 400 Freeze-Fracture Apparatus (Balzers Union, Hudson, NH) at a stage temperature of −80°C for 30 min and then rotary coated with platinum at a 25° angle and with carbon at 60° or 90° angles. Critical point-dried specimens were metal coated in the same fashion, but at 25°C. Replicas were separated from the glass by dissolving the coverslip in 25% hydrofluoric acid, washed in distilled water, and picked up on carbon-formvar coated copper grids.

### Preparation of Actin Gels for Electron Microscopy

Gels composed of purified rabbit skeletal muscle actin and macrophage actin-binding protein were assembled on bovine serum albumin–polylysine ($M_r$ 20,000)–coated copper grids at 37°C and then prepared for electron microscopy as previously described (30).

### Preparation of IgG Antibodies for Immunohistochemistry

The specificity of a polyclonal goat anti-rabbit lung macrophage actin-binding protein IgG used in this study has been documented previously (36). Anti-rabbit skeletal muscle actin IgG was made in rabbits by injecting 1 mg of glutaraldehyde fixed (21) F-actin into multiple subcutaneous sites followed 2 wk later and at subsequent 2-wk intervals with 0.5 mg of this fixed f-actin. The specificity of the immune serum was determined by the immunoblotting electrophoretic technique of Towbin et al. (39). The left side of Fig. 1 shows carbon-stainable protein transferred to nitrocellulose paper when a sample containing 300 μg of total macrophage protein was electrophoresed through a polyacrylamide gel in the presence of dodecyl sulfate (23). The right side of Fig. 1 shows that the IgG in the serum labels only the actin polypeptide. The gel was overloaded with protein to demonstrate the complete lack of cross-reactivity with minor cell components.

All immune IgGs were affinity purified. 20 mg of rabbit skeletal muscle actin or 10 mg of rabbit lung macrophage actin-binding protein was covalently coupled to CNBr-activated Sepharose beads. Specific IgGs were purified from a 45% ammonium sulfate precipitate of serum by dialysis of the precipitate with phosphate-buffered saline (PBS) and by continuous recycling of the sample through the affinity column for 4 h. The columns were washed with PBS until the optical density of the eluted fractions at 280 nm was zero. Bound IgG was eluted with 0.2 M glycine–HCl buffer, pH 2.7. The pH of eluted fractions was immediately adjusted to 7.0 with 1 M phosphate buffer, pH 7.5, and the IgG-containing fractions were dialyzed against PBS containing 0.02% sodium azide. Affinity-purified IgGs were stored at −70°C.

### Preparation of IgG-coated Colloidal Gold Particles

5-nm colloidal gold particles were prepared by the phosphorous reduction method of Faulk and Taylor (13; see also references 15, 35) except that petroleum ether was used instead of diethyl ether. The gold particles were coated with protein immediately after preparation to prevent their fusion into larger particles.

The pH of the colloidal gold–containing solution was adjusted to 9 with 0.2 M $K_2CO_3$. To 20 ml of the gold suspension, 1.2 mg of affinity-purified goat anti-rabbit or rabbit anti-goat IgG was added with stirring. The IgG was dialyzed into 2 mM sodium borate buffer, pH 9.0, and centrifuged at 100,000 *g* for 1 h at 4°C before addition to the gold solution. The IgG–gold solution was stirred for 5 min at room temperature and the particles stabilized by the addition of 8% bovine serum albumin and 5% polyethylene glycol ($M_r$ 20,000) to final concentrations of 1 and 0.05%, respectively.

Stabilized gold particles were collected by centrifugation at 60,000 *g* at 4°C and the pellet was suspended in 1/20 of its original volume in 0.15 M NaCl, 20 mM Tris-HCl, pH 8.2 containing 10 mg/ml bovine serum albumin (BSA) (10, 16). Aggregates were removed by centrifugation of this suspension for 5 min in an Eppendorf microcentrifuge (15,000 *g*) at 4°C and sodium azide was added to give a final concentration of 0.02%. IgG–gold, depleted of aggregates by centrifugation for 5 min in the Eppendorf

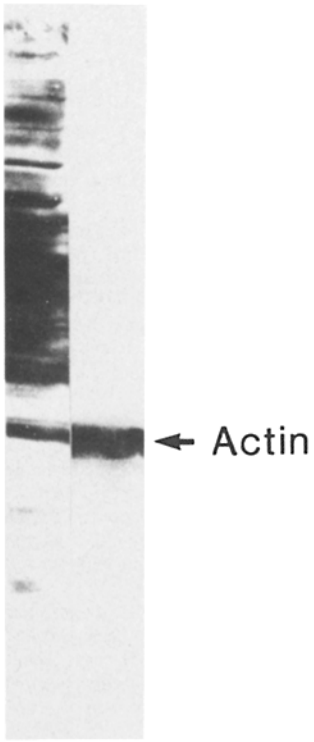


*Figure 1.* Specificity of anti-rabbit skeletal muscle actin antibodies against actin in rabbit lung macrophages demonstrated in electrophoretic immunoblots. (*Left*) India ink stain (17) of a blot of 300 μg of total macrophage proteins electrophoresed through a 5–15% polyacrylamide slab gel in the presence of SDS and then transferred to nitrocellulose. The gel was overloaded to enrich for "possible" minor contaminants. (*Right*) Actin labeling in an identical transfer as in the left lane after incubation with rabbit anti-actin IgG followed by goat anti-rabbit IgG conjugated to horseradish peroxidase (39). The actin polypeptide is indicated.

microcentrifuge, was diluted either 1:10 or 1:20 with 0.15 M NaCl containing 20 mM Tris and 1% BSA, pH 8.2, just before staining of the cytoskeletons.

## *Labeling of Macrophage Cytoskeletons and of Gels Made with Purified Actin and Actin-binding Protein*

***Antibodies.*** Cells permeabilized with Triton X-100 as described above were fixed with 1% glutaraldehyde in PHEM buffer (33) for 10 min. Unreacted aldehydes were blocked by immersion of coverslips into a 10-mM phosphate buffer, pH 7.0, containing sodium borohydride, 1 mg/ml, for 10 min. Individual coverslips were transferred to wells of a 96-well vinyl assay plate (Costar, Cambridge, MA), covered with 30 μl of 10 μg/ml affinity-purified IgG, and incubated between 2 and 12 h at 4°C and then for 1 h at 37°C. They were then washed five times with 0.15 M NaCl, 10 mM Tris, 1% BSA solution, the final wash solution was removed, and 30 μl of IgG–gold particles was added for 1 to 4 h at 37°C. Gold particles were used at dilution of 1:10 and 1:20 in all experiments (vol/vol). Nonspecifically bound particles were removed with five washes of 0.15 M NaCl, 20 mM Tris, 1% BSA solution, followed by five washes of PBS. The coverslips were then fixed for 10 min at room temperature with 1% glutaraldehyde–0.2% tannic acid, 10 mM sodium phosphate buffer, pH 7.4, and washed for 20 min in distilled water. They were then rapidly frozen and freeze dried or dehydrated with ethanol, critical point dried from $CO_2$, and metal coated.

***Myosin Subfragment 1.*** Myosin subfragment 1 was prepared from rabbit skeletal myosin as described by Margossian and Lowey (28). Cytoskeletons were incubated for 10 min at 25°C with 2 mg/ml of myosin S1 in PHEM buffer containing 10% glycerol. The cytoskeletons were washed for 10 min in PHEM buffer to remove unbound myosin S1. They were fixed and prepared for the electron microscope as described above.

***Electron Microscopy.*** Grids were examined and photographed at tilt angles offset ± 10° from horizontal at 80 and 100 kV in a JEOL 1200-EX electron microscope.

## *Quantitation of Actin Filament Length and Concentration, and Angles Formed by Intersecting Filaments*

The lengths of actin filaments between filament intersections and the concentration of actin filaments in the cortex of cytoskeletons were determined from paired electron micrographs as described by Niederman et al. (30). Briefly, paired micrographs were aligned on a GTCO digitizing pad and identical points on each micrograph entered into the memory of a PDP 11/73 Digital computer in similar fashion to that described previously (30). To measure the filament concentration in the cortex of a cytoskeleton, all of the filaments in a cytoskeletal volume were digitized. An area of the cytoskeleton that included all the filaments was defined and then converted to a volume by using the low and high points (in the vertical or Z-axis) determined for the filament ends in that area. The sum of all filament lengths within this volume was then calculated and then converted into actin filament concentration based on 370 actin subunits per micrometer of filament length (18). This volume could be subdivided into smaller sections (serially sectioned along the Z-axis) using the computer and filament concentrations in these sections determined. Filaments within 10 nm (the diameter of a single actin filament after metal coating) of each other were defined as intersecting filaments. Once intersections were established, the length of filaments between two points of intersection was measured.

Four types of filament intersections observed in electron micrographs of cytoskeletons were defined.

(*a*) X-shaped intersections. Since filaments composing the cytoskeleton are relatively straight, X-junctions are definable by four angles that total 360°. Furthermore, these four angles must either be right angles, and therefore all equal, or else not equal, being definable as two acute and two obtuse angles. In the latter case, both the acute angles and the obtuse angles are equal to each other, and 180° minus the acute angle defines the obtuse angle. More than two filaments may also join in space forming a multiple intersection. These complex junctions were considered aggregates of X-shaped intersections when tabulating the results.

(*b*) T-shaped or near T-shaped configurations in which one filament ends along the side of another filament forming three angles. The two smaller angles total 180° and, since one of the filaments is a straight line crossing the intersection, the third "angle" is 180°.

(*c*) Y-shaped filament junctions in which one filament ends on the side of another filament, as in the case of the T's, except that this filament exhibits a bend which is convex with respect to the intersecting filament.

(*d*) Parallel or near parallel side-by-side filament alignments.

The angle between intersecting filaments was determined by entering points on the two intersection filaments away from the intersection point and the points of filament intersection. The angle of vectors describing intersection of the lines defined by the recorded points was calculated by the computer. The following angles were determined at the four types of intersections: (*a*) the right or acute angle of X's and T's; (*b*) the largest angle of the Y's; and (*c*) the number of parallel filament intersections relative to the total filament intersections. The relative distribution of all intersections was quantitated in defined volumes.

## *Quantitation of Cell and Cytoskeleton Heights in Electron Micrographs*

Topological maps of cells and cytoskeletons prepared from macrophages were determined using the computer-based system described above. The data was entered into the computer by digitizing the cell surface using low power (5,000–8,000× enlargements) stereo micrographs. Surface points were digitized across the cell near the cell center, by transecting it perpendicular to the tilt axis of the micrographs. Surface points were entered into the computer along this line. When the topology of intact cells was determined, height data was categorized into the type of surface structure, as either the general surface or microvilli and veils extending upward from this surface.

## *Quantitation of Gold Labeling in Electron Micrographs*

Cortical regions of 1 $\mu m^2$ of the residues were analyzed from photographically enlarged prints. The regions analyzed were all within 2 μm of the cell edge and within spread lamellae. Using the stereo viewer, the total number of gold particles in the 1-$\mu m^2$ area, the total number and type of filament intersections, and the number of gold clusters associated with either filament junctions and ends, or along their length were counted. For labeling with anti-actin IgG and anti-IgG-gold, the total number of filament associated particles was divided by the total filament length in μm to yield the number of gold particles per μm of filament.

## *Effect of Detergent Extraction on the Distribution of Macrophage Proteins*

Monolayers of macrophages were prepared by attaching the cells to 5.0-cm plastic petri dishes and incubating them as described above for cell attach-

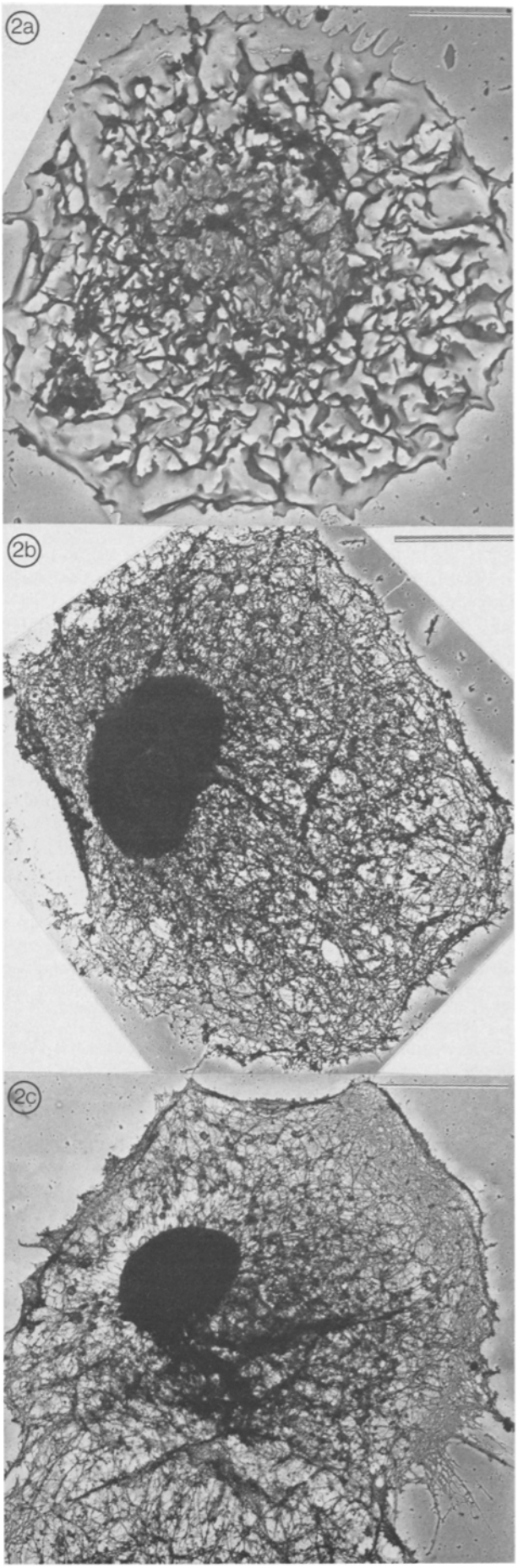


ment and spreading. Cells were extracted with 0.5 ml of 0.75% Triton X-100 in PHEM solution. The total cell protein was determined in separate dishes by Folin-Phenol method (27). After 2 min, the supernatant fluids from Triton-permeabilized cells were removed with pasteur pipets and divided in half for determination of total protein and for analysis of their polypeptide composition by electrophoresis in 5-15% gradient polyacrylamide slab gels in the presence of SDS (23). Similarly, the amount of protein remaining in the insoluble cytoskeleton and its polypeptide composition were analyzed by solubilizing the insoluble residue remaining on the petri dish with boiling 1% SDS in the gel sample buffer of Laemmli (23). Each measurement was done in triplicate. To remove residual Triton X-100 which could interfere with protein assays, protein solutions were mixed with an equal volume of 10% TCA solution, and the protein precipitates were washed with diethyl ether/ethanol (3:1, vol/vol) (32). In some experiments, the concentrations of extractable, total, and monomeric actin were measured by the DNAase I inhibition assay in the presence and absence of 1 M guanidine-HCl (5, 8).

The amounts of actin and actin-binding protein polypeptides in the insoluble and soluble phases were determined densitometrically from the relative intensity of the Coomassie Blue-stained proteins on the polyacrylamide gels. The Coomassie Blue staining of actin and actin-binding protein was directly proportional to the concentration of each protein applied (19). The precise migration of each polypeptide was determined by electrophoretic transfer to nitrocellulose paper and identification with anti-actin or anti-actin-binding protein antibodies (39).

To look for the release of long actin filaments from cells permeabilized with detergent, a drop of the supernatant was applied to carbon-formvar coated grids. The grids were glow discharged before addition of the protein-containing supernatant. The grid were negatively stained with 1% uranyl acetate and viewed in the electron microscope.

## Results

### Appearance of Macrophages during Attachment and Spreading

When rabbit pulmonary macrophages attach to a surface at 37°C, they change within minutes from a spherical to a flattened morphology. Observed in the light microscope, spreading occurs by the outward flow of a thin lamella that excludes the majority of cellular organelles and granules and, in general, occurs equally around the cell periphery. By 10 min, the peripheral lamellae have spread 4–8 μm from the cell body. Although these lamellae appear completely flattened in the light microscope, the upper cell surface of spreading cells is highly convoluted. The complexity of this surface can be appreciated in low magnification micrographs of intact cells. Fig. 2 *a* shows a representative cell fixed after incubating for 10 min at 37°C and then prepared for the electron microscope by rapid freezing and freeze drying. Its upper surface, as well as its margins are replete with large membrane protrusions, microvilli, and veils. Veils extend upward 0.7–3.0 μm from the bulk of the cell which is in turn elevated on average 0.3–0.6 μm off the substrate (Fig. 3). We have initially examined the structure of actin filaments in

*Figure 2.* Electron micrographs comparing the structure of an intact macrophage with cytoskeletons prepared by either freeze or critical point drying. (*a*) Electron micrograph showing the morphology of a spread macrophage after incubation at 37°C for 10 min, fixation with 1% glutaraldehyde–0.2% tannic acid, and preparation for electron microscopy by rapid freezing and freeze drying. Bar, 5 μm. (*b*) Electron micrograph showing the morphology of a spread macrophage after incubation at 37°C for 10 min, Triton X-100 extraction, and preparation for electron microscopy by rapid freezing and freeze drying. Bar, 5 μm. (*c*) Electron micrograph showing the morphology of a spread macrophage after incubation at 37°C for 10 min, Triton X-100 extraction, and preparation for electron microscopy by critical point drying. Bar, 5 μm.

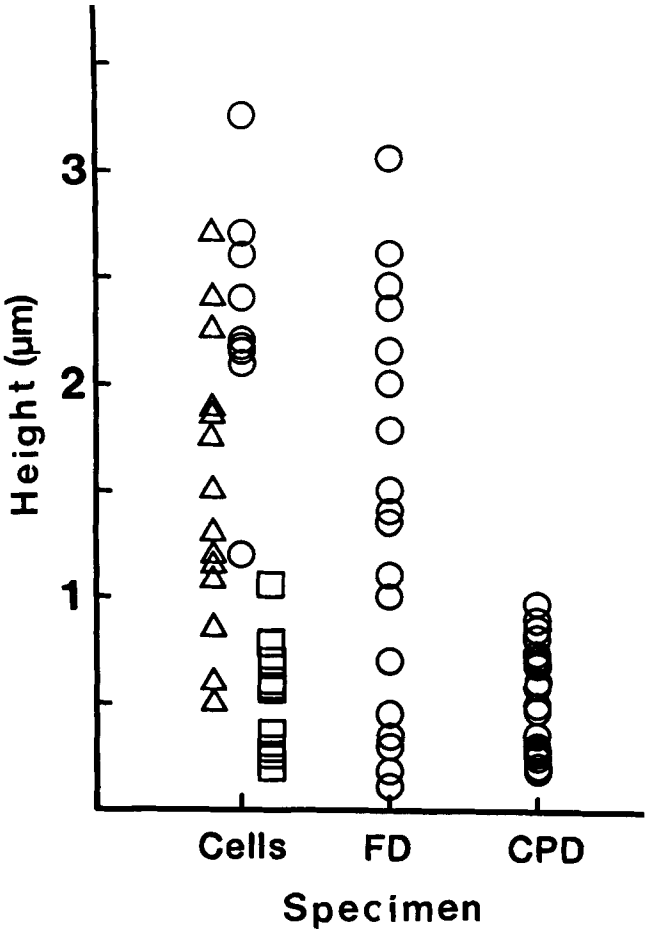


*Figure 3.* Scattergram plot comparing the three-dimensionality of intact cells and of cytoskeletons prepared by either freeze or critical point drying (*FD* and *CPD*, respectively). The height of the surface structure measured in intact cells has been related to the type of structure present on the cell surface: triangles indicate microvilli-like extensions; circles indicate surface veils or ruffles; and squares indicate the top cell surface from which these extensions project. Since these structures cannot be clearly categorized in the freeze- and critical point-dried cytoskeletons, only the variation in heights have been plotted.

cells incubated for 10 min, at which time most macrophages were in the process of spreading on the grid surface. Our studies focused on the large regions of hyaline cytoplasm parallel to the substrate.

### *The Structure of Cortical Filaments in the Lamellae of Freeze- and Critical Point-dried Macrophage Cytoskeletons*

The cortical cytoskeleton of the macrophage, which ranges in thickness from 0.2 to 0.5 μm, is completely filled with a dense network of 10-nm diameter filaments. These filaments also invest the cell body with a thin mantle. In both freeze- and critical point-dried specimens, intact cytoskeletons of entire cells are preserved (Fig. 2 *b* and *c*) after permeabilizing the cells with detergent and preparing them for observation in the electron microscope. However, cytoskeletons prepared by freeze drying (Fig. 2 *b*) were considerably more three-dimensional than those prepared by critical point drying (Fig. 2 *c*), indicating considerable collapse of filaments during critical point drying relative to freeze drying. To evaluate the three-dimensionality of these two preparations, we quantitated the height of cytoskeletons at various points along their surface and compared these to those derived from the surface of intact cells. The data plotted in Fig. 3 clearly demonstrates that only freeze-dried cytoskeletons preserved cell-like three-dimensionality. Fig. 4, *a* and *b*, compares at higher magnification the three-dimensional organization of cortical filaments in cytoskeletons prepared by freeze drying and critical point drying, respectively, and Fig. 5 *a* shows the structure of filaments in freeze-dried cytoskeletons at high magnification. Cortical filaments were much more uniform in diameter along their length in the freeze-dried cytoskeletons. Further, the diameter of filaments was more variable in the critical point-dried cytoskeletons. As quantitated below, critical point-dried filaments collapse downward, in a fashion comparable to the squeezing of an accordion, and aggregate sideways. However, in both cases, the most distinguishing feature of the network is that it is composed of short filaments that are interconnected at their ends; i.e., free filament ends are rarely seen within the body of the network because the filaments end by abutting the side of another filament. Free ends, which are easily visualized in the paired micrographs, occur only in filaments that extend upward and downward from the body of the network.

The different types of filament intersections are revealed at higher magnification in the stereo-paired micrographs of freeze- and critical point-dried cytoskeletons and are of four morphological types. End-to-side intersections predominate: 70% of total intersections were of this type. These are further divisible into Y-shaped configurations, in which 120–130° angles are formed by intersecting filaments (Fig. 6), and T-shaped intersections, composed of perpendicularly branching filaments. Y's and T's represented 35.6 and 34.6% of the total intersections ($n$ = 482), respectively. T's and Y's appeared to represent similar filament interactions, except that Y's result when one filament is bent at the attachment point of the other. The distribution of branch angles with one peak near 90° and another at 120–140° is in agreement with the equal distribution of T- and Y-shaped intersections in these cytoskeletons. Filaments also overlap to form X intersections (14% of the total junctions).

Filament bundles are not observed in the cortex of these flattened cells, although filaments in ruffles can be seen to become somewhat aligned with the cell margins. However, a number of filament intersections, 13% of the total, are formed by the convergence and parallel alignment of two filaments. In many of these cases, filaments coming together are bent and/or twisted where they align. Filaments run in parallel for only short distances and then end or branch off. Some filaments oriented in parallel are also seen in filopodia extending from the edges of the cortical lamellae.

Although critical point-dried cytoskeletons are not as three-dimensional across their surface, the arrangement of filaments near the cell margins is quantitatively similar to that in freeze-dried cytoskeletons. The critical point-dried networks do display, however, a somewhat different distribution of filament intersection types. Filaments intersect most frequently as T-shaped junctions. Of the total intersections in critical point-dried cytoskeletons, 60% are T's ($n$ = 486); Y and X intersections represent 22 and 13% of this total, respectively. Correspondingly, the filament branch angle

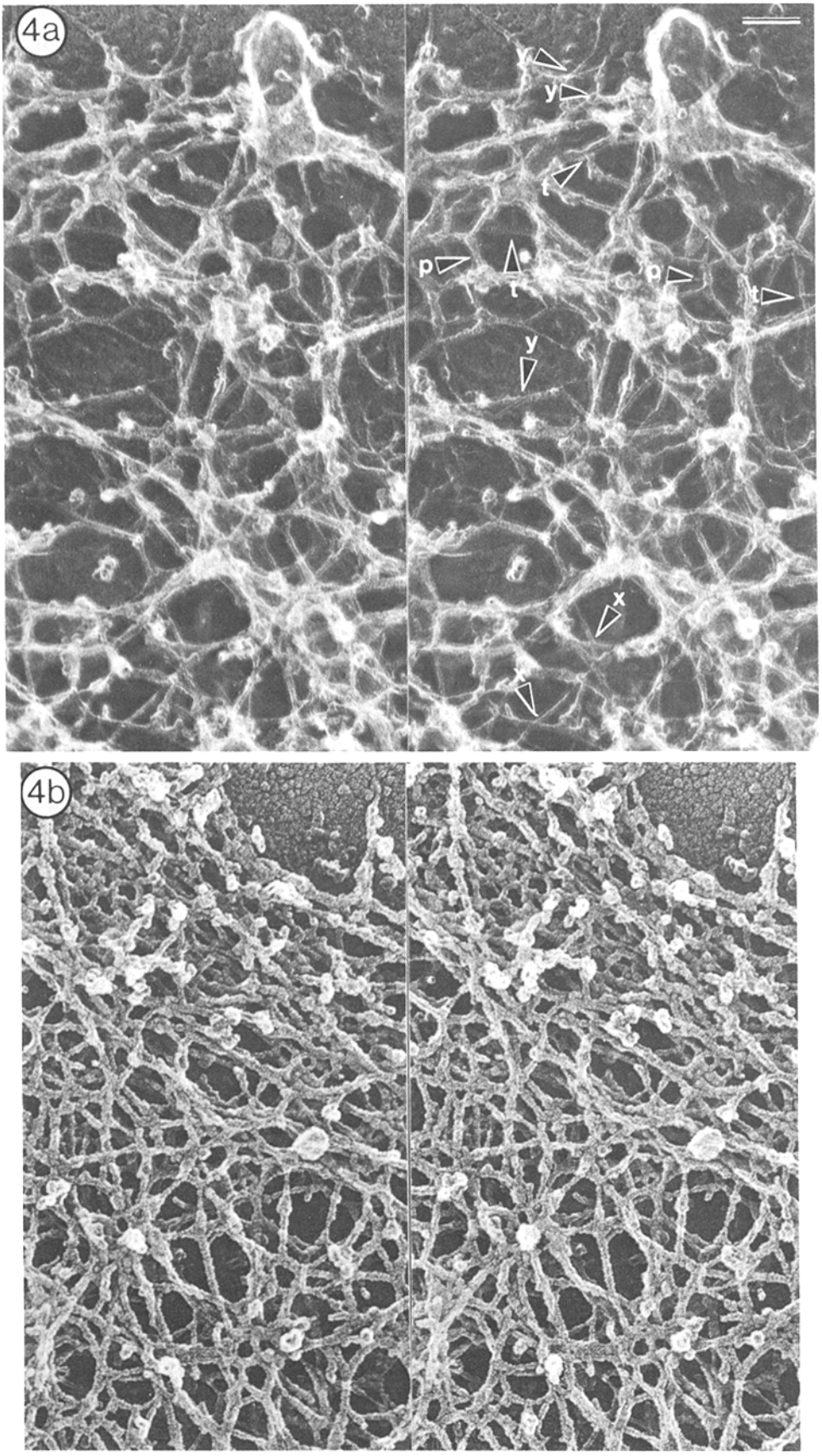


*Figure 4.* (*a*) Stereo electron micrographs showing the morphology of the cortex of a macrophage cytoskeleton prepared by freeze drying. (*b*) Stereo electron micrographs showing the morphology of a spread macrophage cytoskeleton prepared by critical point drying. The different types of filament intersections found in the cortex of freeze-dried macrophage cytoskeleton are indicated. Representative examples of each type of junction are labeled as follows: T-shaped (*t*'s and *arrows*) and Y-shaped (*y*'s and *arrows*) branches, x-shaped filament intersections (*x*'s and *arrows*), and parallel filament intersections (*p*'s and *arrows*). Bar, 0.1 μm.

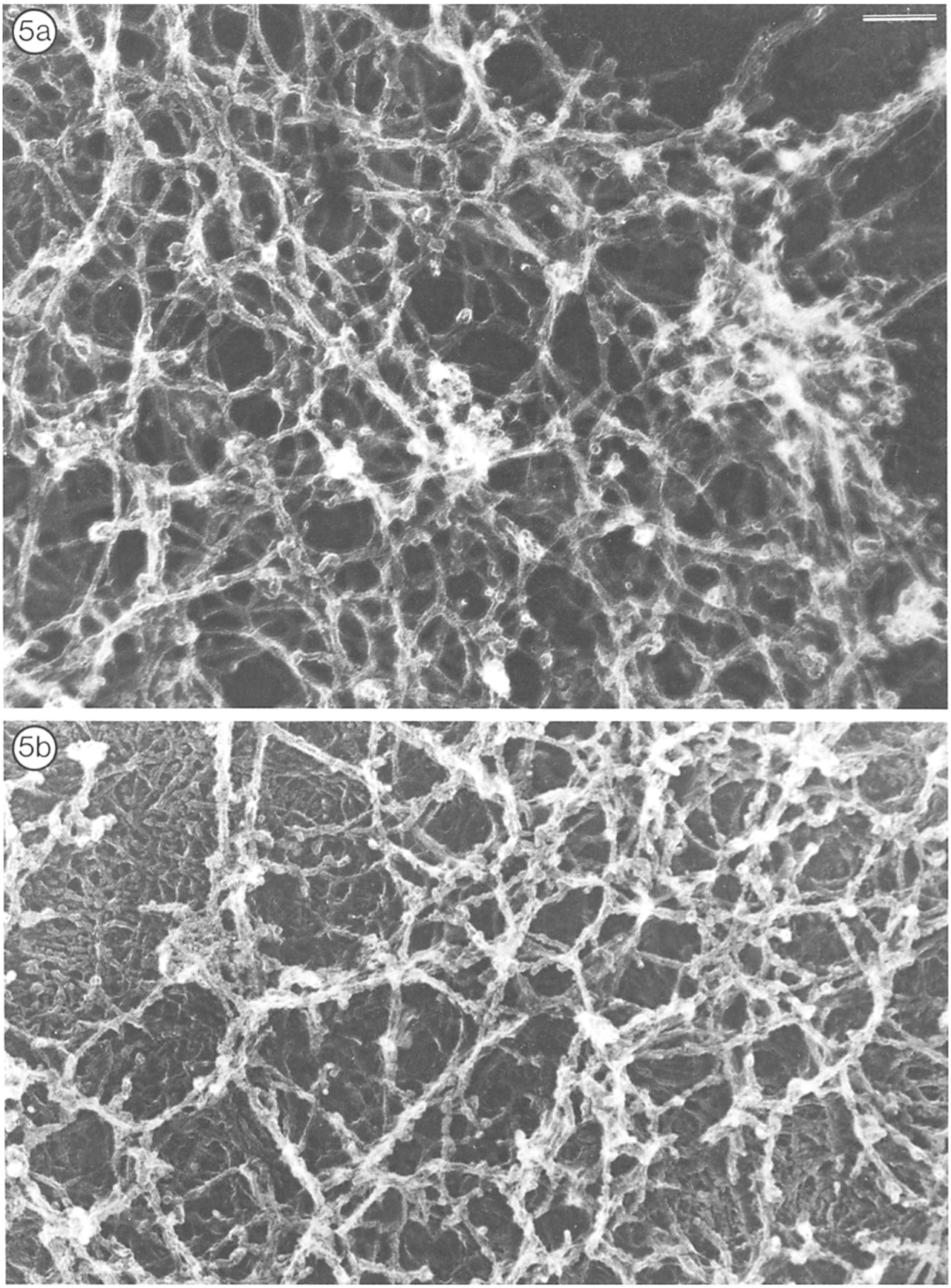


*Figure 5.* (*a*) High magnification micrograph displaying the cortex of freeze-dried macrophage cytoskeleton. The light areas near the margin are points where the filament network forms veils. Bar, 0.1 μm. (*b*) Representative electron micrograph of actin assembled in the presence of actin-binding protein at a molar ratio of 1 actin-binding protein to 50 actin monomers as described previously (32) except that the sample was frozen on a helium-cooled copper block and freeze dried.

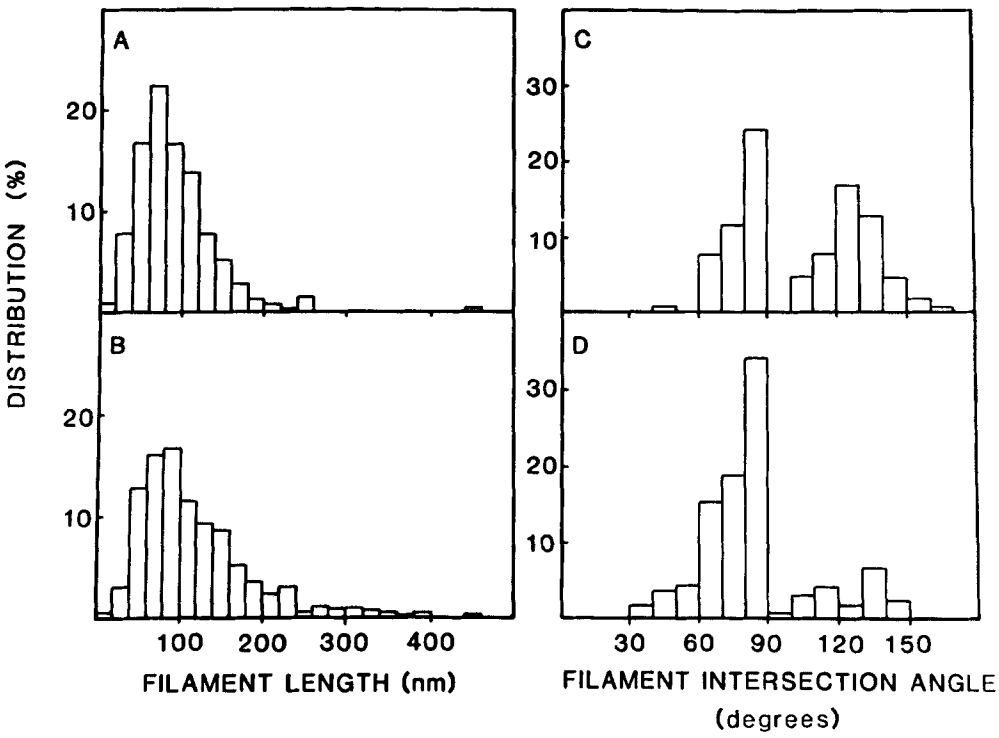


*Figure 6.* Histograms describing the length of actin filaments between points of intersection (*A* and *B*) and the angles formed at points where filaments intersect (*C* and *D*). *B* and *D* were quantitated from critical point-dried cytoskeletons. 1,163 segments between filament intersections were measured in *B* and 500 branch angles in *D*. *A* and *C* represent freeze-dried cytoskeletons. 424 filament segments were measured in *A* and the 500 filament angles in *C*. These data were obtained by computer-assisted quantitative morphometry of 20 volumes from 10 cells from paired electron micrographs as described in Materials and Methods.

distribution was Gaussian with a major peak value of 90°. A minor fraction of overlap angles clustered between 100° and 150° and represented the branching angle of Y-shaped intersections. Therefore, Y intersections are apparently converted to T junctions when the samples are dried from $CO_2$, a finding that may be related to network shrinkage caused by this technique.

The filament length between filament intersections, the angle formed by filaments when they form X, T, or Y intersections, and the concentration of actin filaments in a region of the cell were quantitated from paired micrographs of both freeze- and critical point-dried cytoskeletons. Fig. 6 shows histograms comparing the length distribution of filaments between branch points (*A* and *B*) and of the angle of filament branching (*C* and *D*) in the two types of preparations. The mean distance between filament intersections was 91 ± 47 nm ($n$ = 424) and 118 ± 72 nm (± SD, $n$ = 1,163) for freeze- and critical point-dried preparations, respectively. Of the two, the interfilament branch length in the freeze-dried samples had a more uniform length distribution. Since free filament ends are rarely observed, the end-to-end length of individual filaments could not be assessed morphometrically.

The concentration of 10-nm filaments calculated for the cortical cytoskeleton varied depending on the boundaries used in this analysis. In general, when a representative cytoskeleton was serially sectioned using the computer along the vertical axis from the bottom of the cell to its top, concentrations calculated for the edge regions were much lower than in those from the cytoskeleton middle. This is because only a small number of filaments enter and end in these regions. However, when concentrations were calculated near the middle of the network, higher and more uniform concentrations were obtained. The average filament concentration within the lamellae calculated for the mid-section of freeze-dried cytoskeletons was 12.3 ± 1.6 mg/ml ($n$ = 6) and values as large as 16.5 mg/ml were determined. On the other hand, filament concentrations from the mid-point of critical point-dried cytoskeletons were much more heterogeneous, ranging from 4.48 to 22.9 mg/ml and averaging 12.5 ± 6.7 mg/ml ($n$ = 10), due to regional collapse and aggregation during drying.

### *Composition of Cortical 10-nm Filaments*

The majority of these filaments are actin because (*a*) they have the same diameter as purified actin filaments prepared and observed by identical techniques (22, 30); (*b*) 80–85% of them labeled specifically with anti-actin IgGs as described below; and (*c*) they decorate uniformly with myosin subfragment 1, forming arrowhead or rope-like structures in freeze-dried specimens (Fig. 7). The ability of the anti-actin IgG antibody and gold particles coated with anti-IgG to label actin filaments was tested in a gel made with skeletal muscle actin and actin-binding protein. Actin filaments were heavily and uniformly labeled by this procedure (not shown).

Fig. 8 *a* shows a representative electron micrograph of a macrophage cytoskeleton after labeling for actin with rabbit anti-skeletal muscle actin IgG and 3–5-nm gold particles coated with goat anti-rabbit IgG. Most cortical filaments are greatly thickened compared with cortical filaments from unlabeled cytoskeletons (compare filaments in Fig. 8 *a* with those in its inset). The inset shows that absorption of the anti-actin IgG with actin filaments before staining the cytoskeletons abolished gold labeling of the cortical cytoskeleton. Quantitative morphometry revealed that 78% of the individual 10-nm fiber units were labeled along their length with gold particles. Labeling was equivalent to one IgG-coated gold bead for every 2–3 monomers of actin in the filaments, indicative of uniform labeling of actin filaments. Not all cortical filaments, however, were labeled. A group of 10-

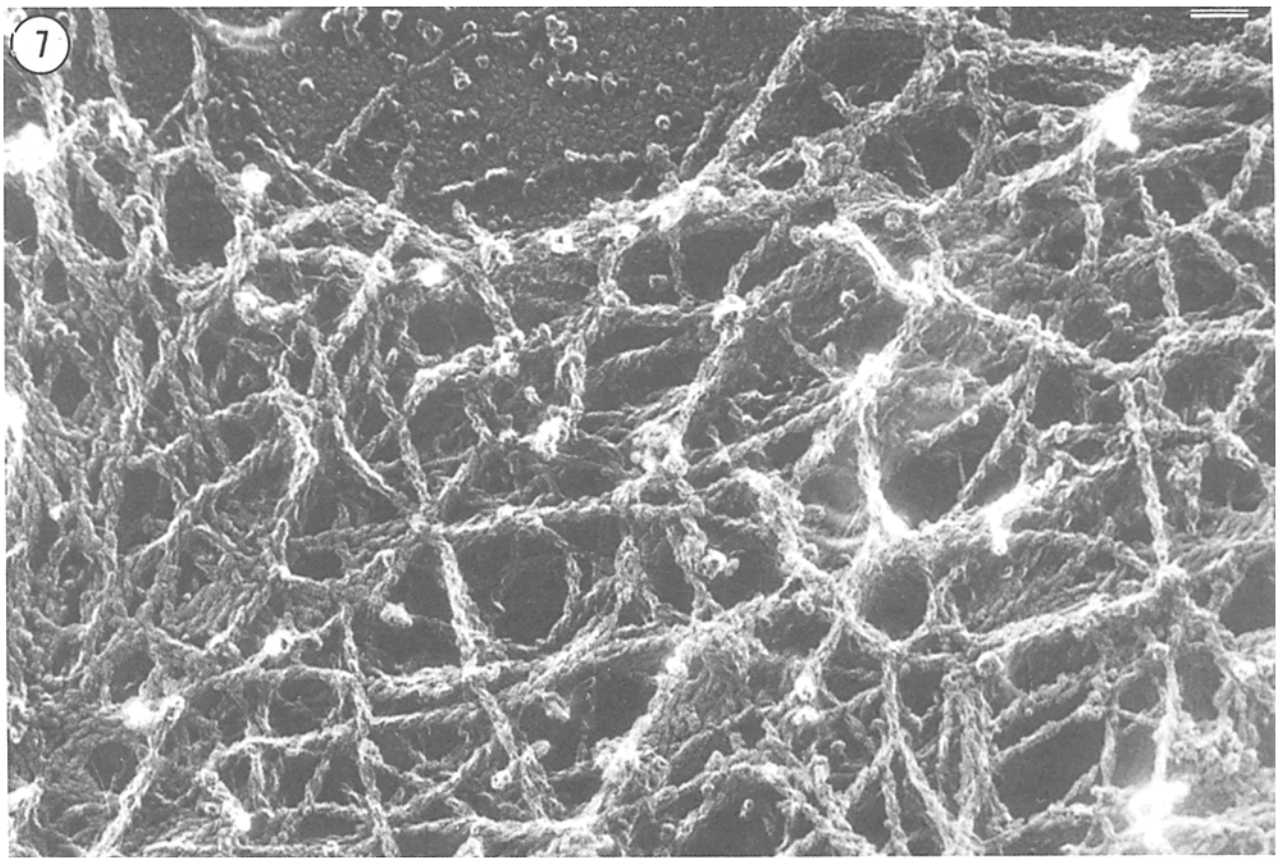

*Figure 7.* Representative electron micrograph of the cortex of a macrophage cytoskeleton after incubation with myosin subfragment 1. Bar, 0.1 μm.

nm filaments did not label, and unlabeled filaments with small diameters are revealed. The long, straight 10-nm diameter elements may be intermediate filaments. Compared to the labeling of purified actin filaments, cytoskeletal actin filaments labeled less efficiently. This may be caused by masking of antigenic sites in cells by other proteins adherent to actin filaments, by the differences in actin isoforms between skeletal and macrophage actin, and possibly by a lower affinity of the antibodies for the macrophage actin. It was not possible to estimate the proportion of actin after labeling with myosin subfragment 1. Although the vast majority of cortical filaments label with subfragment 1, such treatment alters the overall architecture of the cortical network by increasing in the spacing of the network from 0.1 μm to 0.4–0.5 μm. Since large numbers of short, decorated filaments are observed on the substrate after myosin S1 treatment, subfragment 1 must competitively dissociate cross-linking proteins from the sides of the filaments, causing them to fall out of the cytoskeleton.

### *Localization of Actin-binding Protein in the Macrophage Cytoskeleton*

We have previously shown that actin-binding protein promotes the perpendicular or near perpendicular branching of actin filaments in samples prepared for the electron microscope by critical point drying (30). As shown in Fig. 5 *b*, actin-binding protein–actin prepared by freeze-drying looks quite similar to the critical point–dried proteins. Furthermore, because of the structural similarity of this reconstituted actin gel to actin filaments present in the cortex of macrophage cytoskeletons (compare Fig. 5 *b* with *a*), we have investigated in the electron microscope the location of actin-binding protein molecules in macrophage cytoskeletons.

As shown in Figs. 8 *b* and 9, when actin-binding protein was visualized in the electron microscope with IgG and anti-IgG-coated gold beads, the majority of gold label occurs in aggregates, either in small clusters 20–40 nm in diameter, having three or more gold beads in them, or, less commonly, in extended linear chains of gold beads. The cluster pattern of labeling is consistent with a recent report describing patchy staining of thin sections of fibroblasts with anti-filamin antibody (25). Filamin is immunologically cross-reactive with actin binding protein. In this case, as opposed to the labeling of actin with antibodies, the gold labeling procedures did not appear to greatly obscure the three-dimensional structure of the cytoskeleton. Table I summarizes the distribution of gold particles in freeze-dried cytoskeletons. Label was found almost exclusively at high angle filament intersections and without preference for the type of filament intersection. 38% of these intersections were decorated with gold clusters. 25% of all filament ends that extended upward and downward from the main bulk of the network were also labeled. These may represent points where actin-binding protein is attached to membrane components as has been reported for platelet actin-binding protein (14, 31). This labeling, however, represented only 3% of the total cytoskeletal labeling. The insert of Fig. 8 *b* shows the

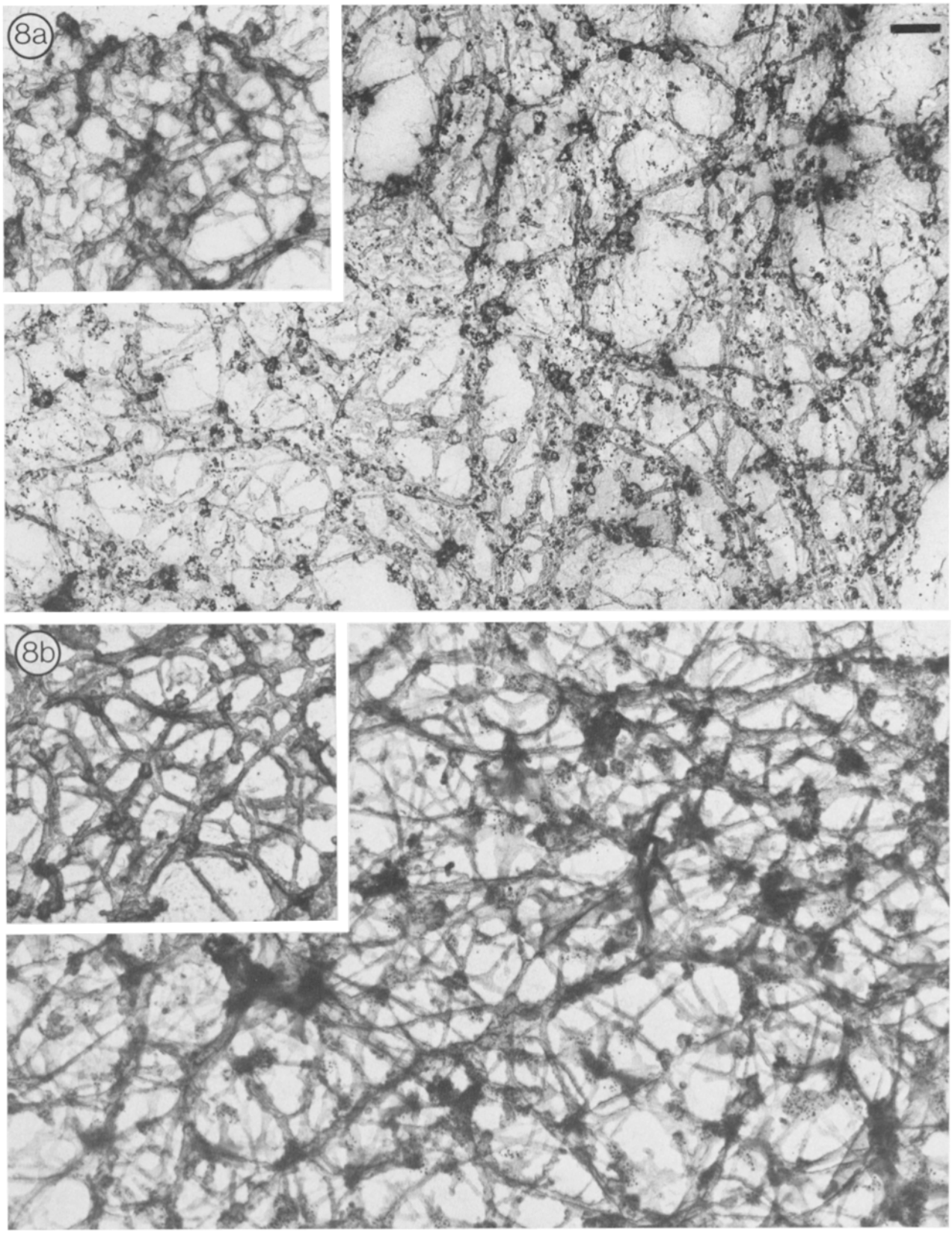


*Figure 8.* (*a*) Electron micrograph showing the distribution of actin in the cortex of a macrophage cytoskeleton. The cytoskeleton was incubated with rabbit anti-actin IgG and colloidal gold particles coated with goat anti-rabbit IgG. (*Inset*) Control for *a*. F-actin absorbed anti-actin IgG was substituted for anti-actin IgG. (*b*) Representative electron micrograph showing the distribution of anti-actin-binding protein label in the cortex of a macrophage cytoskeleton prepared by freeze drying. As can be seen, the gold is found in clusters. (*Inset*) Same as *b* except primary IgG was preabsorbed with actin-binding protein. Bar, 0.1 μm.

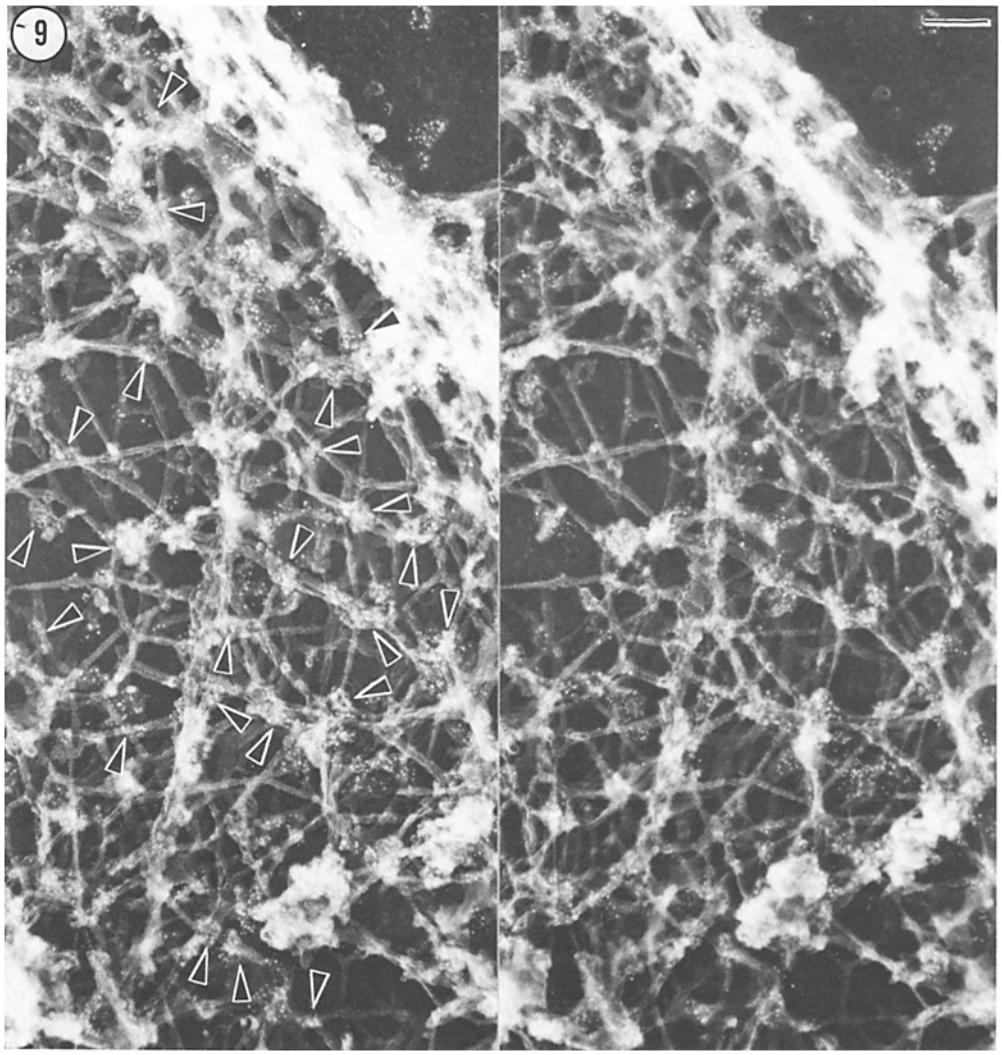

*Figure 9.* Stereo micrographs demonstrating the localization of actin-binding protein at points where actin filaments intersect and at the ends of actin filaments in the cortex of a macrophage cytoskeleton. Representative gold-decorated filament intersections and filament ends that point upward and downward are labeled with the arrows. Bar, 0.1 μm.

specificity of anti-actin-binding protein labeling. Absorption of anti-actin-binding protein with actin-binding protein abolished gold labeling of the cytoskeletons.

Gold clusters also characterized the labeling of an actin gel made with actin-binding protein and reacted with anti-actin-binding protein IgG and 2–5-nm IgG-coated gold particles. Compared to the labeling frequency of macrophage cytoskeletons, a higher percentage of the total intersections (75%) were decorated with gold clusters (Table II).

### *Distribution of Actin and Actin-binding Protein in Triton-soluble and -insoluble Phases*

Table III shows the distribution of macrophage actin and actin-binding protein between the soluble and insoluble frac-

*Table I. Distribution of Gold Clusters in Macrophage Cytoskeletons Labeled with Anti-Actin-binding Protein IgG and Immunogold Particles*

| | | Intersections | | | | | | | Other types of gold labeling | | |
|---|---|---|---|---|---|---|---|---|---|---|---|
| | | T's | | X's | | Y's | | % of Total labeled | Filament sides | Filament ends* | |
| Cell | Area analyzed | Total | Labeled | Total | Labeled | Total | Labeled | | Clusters | Total | Labeled |
| 1 | 0–1 μm | 81 | 35 | 28 | 13 | 51 | 18 | 41 | | | |
| 2 | | 60 | 22 | 20 | 05 | 37 | 12 | 33 | | | |
| 3 | | 39 | 14 | 06 | 01 | 21 | 09 | 36 | | | |
| | Total | 180 | 71 | 54 | 19 | 109 | 39 | 38 | 2 (1.4%) | 24 | 6 (25%) |
| 1 | 1–2 μm | 81 | 33 | 36 | 11 | 67 | 26 | 38 | | | |
| 2 | | 65 | 30 | 16 | 04 | 34 | 14 | 42 | | | |
| 3 | | 70 | 22 | 20 | 08 | 48 | 16 | 33 | | | |
| | Total | 216 | 85 | 72 | 23 | 149 | 56 | 38 | 3 (1.8%) | 16 | 4 (25%) |

* Filament ends are observed only on filaments that appear to be attached to the membrane at the cell bottom or on filaments that end at the top of the cytoskeleton.

*Table II. Distribution of Gold Clusters in an Actin Gel Made with Actin-binding Protein and Labeled with Anti-Actin-binding Protein IgG*

| Volume measured | Filament length in volume | Filament length between intersection | Gold clusters | | Total intersections | Gold clusters at intersections | | |
|---|---|---|---|---|---|---|---|---|
| | | | Total | per μm filament | | Total | T | X |
| $\mu m^3$ | μm | μm | n | n | | % | % | % |
| 0.018 | 17.7 | 0.300 ± 0.200‡ | 49 | 2.8 | 62 | 75 | 77 | 69 |

The molar ratio of actin-binding protein to actin of the sample labeled was 1:100.
* Expressed as % of total cluster labeling.
‡ Mean ± SD.

tions generated by detergent treatment in the presence of 10 mM EGTA. As reported for other cells, actin distributes equally between the insoluble and soluble phases (6). The retention of actin-binding protein in the cytoskeleton fraction was somewhat greater, with 68% in the insoluble cytoskeleton. Actin protein released by detergent (soluble phase) was not assembled into long filaments but was in the form of monomers or very short oligomers. First, no actin filaments were observed in the electron microscope when the supernatant fluid was applied to grids and negatively stained with uranyl acetate. Second, the actin in the supernatant, although present at concentrations well above the critical concentration for polymerization of purified actins (38), did not sediment when centrifuged at speeds which sediment actin filaments (30 psi for 60 min in an Airfuge). Third, using the DNAase inhibition assay, there was no detectable difference in the amount of actin solubilized by Triton X-100 whether assayed in the presence or absence of guanidine–HCl. In a representative experiment, 15.6 ± 2.8 μg of actin was released by detergent from petri dishes containing adherent macrophages (mean ± SD of quadruplicate dishes). When the same supernatants were assayed in the presence of guanidine–HCl, total actin released was 15.3 ± 2.9 μg. These findings suggest (*a*) that the solubilization procedure did not alter the arrangement of actin in the residue by removing preexisting actin filaments; and (*b*) that the majority of actin-binding protein molecules are associated with assembled actin in the cytoskeleton.

## Discussion

An apparently straightforward approach to understanding the molecular structures responsible for the mechanical properties of peripheral cytoplasm is to examine cytoplasm with the electron microscope. This paper describes results of an effort to examine and quantitate at least some of the structural features of the three-dimensional architecture of filaments remaining in the spread lamellae of rabbit lung macrophages after extraction of the cells with Triton X-100 solutions.

The essential conclusions are that the cortical filaments are composed of actin, are present at an average concentration of 10 mg/ml (12.5 mg/ml 10-nm filaments × 80% actin), and are organized into a dense three-dimensional network. Individual actin filaments are relatively short and straight. Actin filaments intersect with one another regularly in three-dimensional space or form connections in which one filament branches from the side of another. Filament intersections at points of crossing occur predominantly at high angles which approach perpendicular. The pore size of the orthogonal actin network is small enough to account for the organelle exclusion appreciated with the light microscope, yet large enough to accommodate the percolation of solutes and solvents within the cell periphery. The relatively short length of the cortical actin filaments predicts that actin filaments alone at the concentrations represented could not contribute much to the viscosity and elasticity of cytoplasm within the lamellae, and that therefore, actin cross-linking proteins, such as actin-binding protein, must carry a large responsibility for these properties. We demonstrated that one such cross-linking molecule, actin-binding protein, previously shown to promote orthogonal branching of F-actin in negatively stained and in critical point-dried samples, and here in quick frozen specimens, localized immunocytochemically at points of actin filament branching, adding further support to the notion that the mechanical behavior of this re-

*Table III. Distribution of Actin and Actin-binding protein in Detergent-permeabilized Macrophages*

| Fraction | Protein | | Actin | | Actin-binding protein | |
|---|---|---|---|---|---|---|
| | μg | %* | μg | % | μg | % |
| Whole cells | 110 ± 23 | 100 | 13.4 ± 2.8 | 12.2 | 0.55 ± 0.1 | 0.5 |
| | | | | %‡ | | %‡ |
| Triton-insoluble cytoskeleton | 47 ± 6 | 43 ± 6 | 6.1 ± 1.0 | 48 ± 8 | 0.48 ± .10 | 68 ± 29 |
| Triton-soluble extract | 63 ± 7 | 57 ± 6 | 6.8 ± 0.8 | 55 ± 6 | 0.22 ± .08 | 32 ± 23 |

Cells spread on the surface of petri dishes were permeabilized as described in Materials and Methods. The % of total protein in actin and actin-binding protein polypeptides was determined by quantitative densitometry of Coomassie Blue–stained polyacrylamide gels after electrophoresis in the presence of SDS. The μg of each individual protein was calculated from the % of each individual protein x μg total protein in fraction.
* % of total protein.
‡ % of an individual protein (μg individual protein in fraction/μg of total individual protein).

gion of cytoplasm derives from a cross-linked actin filament gel.

### *Reliability of Electron Microscopic Images*

Efforts were expended to determine the reliability of the electron microscopic images. First, the effect of detergent extraction on the distribution of cytoplasmic actin and actin-binding protein was assessed. Under the extraction conditions used, about half of the actin was solubilized and the solubilized actin was not in a filamentous form. This finding agrees with previous studies which have estimated that about half of the cytoplasmic actin is not polymerized but is complexed to profilin or other profilin-like molecules (8). Profilin has been purified from rabbit lung macrophages (12).

Second, two methods were used to remove water from the detergent-extracted specimens during preparation for electron microscopy; namely, freeze drying and critical point drying. Although there were notable differences in some details of the structure obtained by the two techniques, the overall conclusions were not affected. The principal discrepancies observed were a greater homogeneity of the cortical actin network in the frozen specimens, suggesting less collapse and aggregation than may have taken place during critical point drying. Further, by directly comparing the topology of freeze-dried cytoskeletons to that of intact cells, it was clear that there was little, if any, collapse in freeze-dried cells. In addition, the freeze-drying method, by providing better resolution of individual actin filaments, revealed that some of the junctions which were interpreted as Y- and T-shaped in the critical point-dried specimens actually were places where filaments aligned side-by-side separated abruptly.

### *Immunoelectron Microscopic Studies*

In macrophage cytoskeletons labeled with anti–actin-binding protein IgG and gold beads coated with anti-IgG and then freeze-dried, gold localized near filament intersections. The evidence indicates that such a localization is not artifactual. First, the pattern of labeling for actin in the cytoskeletons by identical techniques does not show preference for filament intersections. Second, the spacing or pore size of the network was not altered by the antibody and gold treatment, indicating that shrinkage artifacts did not occur, resulting in aggregation of gold particles separated in space before drying.

In orthogonal networks of actin assembled with actin-binding protein in vitro, the distances between fiber overlaps shortens in proportion to the actin-binding protein concentration (30). At the molar ratio of actin to actin-binding protein (100:1) used in the experiment described in Table II, the predicted fiber length between intersections is 346 nm. This prediction assumes an equal distribution of actin monomers on actin-binding protein molecules, 370 actin monomers per micrometer of fiber length (18) and that 78% of the actin-binding protein binds to actin at the concentration used (19). In actin gels labeled to detect actin-binding protein molecules, there was one gold cluster for every 361 nm of actin filament length. This value is very close to the predicted value of 346 nm and indicates a 96% labeling efficiency. The average spacing between intersections was 300 nm. However, only 75% of the fiber intersections in the actin-binding protein and actin network had gold clusters. If the unlabeled intersections are overlaps without cross-links, then the spacing between junctions linked by actin-binding protein molecules would actually be 375 nm. This value is within 4% of the measured average filament length per cluster.

The cortex of the macrophage cytoskeleton contains an actin network which qualitatively resembles the actin gel made with actin-binding protein (Fig. 5 *b*) because of the near-perpendicular intersection of actin fibers. The measured molar ratio of actin to actin-binding protein in the macrophage cytoskeleton (150:1) leads to a predicted spacing between actin filament intersections of 410 nm, yet the average distance measured was 100 nm. The simplest interpretation of this discrepancy is that a significant fraction of filament overlaps in the cortical cytoskeleton are not joined by actin-binding protein molecules. The fraction of fiber intersections labeled for actin-binding protein in the macrophage cortical cytoskeleton (38% of the total) is consistent with this view. If 62% of the overlaps do not contain actin-binding protein molecules, then the actual lattice spacing between actin-binding protein-linked junctions is 260 nm, a value closer to the average spacing of clusters in the cortical cytoskeleton.

The differences in configuration between the macrophage cortical cytoskeletal actin and actin assembled in the presence of actin-binding protein undoubtedly arise from the greater complexity of the cortical assembly. For example, the existence in the cell of structures capable of nucleating actin assembly could lead to more actin fiber entanglement, because these nuclei would preclude a uniform distribution of actin associating with the population of actin-binding protein molecules. Branching from these nucleated filaments would produce a series of mutually interdigitating networks rather than a continuous matrix. It is also self-evident that once a number of filaments are cross-linked by actin-binding protein, causing them to branch at near right angles, a pattern of perpendicular crossovers would be established without a requirement for extensive additional cross-linking, although the extent of cross-linking would affect the elastic properties of the network.

This work represents a four-year investment in new technology for us and we thank Dr. Evarist Feliu for contributing to its early and rather frustrating phase. Ms. Nicole Lee provided invaluable technical assistance early on. We also thank Drs. Dennis Landis and David Begg for their help in quick freezing and Dr. David Begg for checking over our work before submission for publication. We also acknowledge the continuing support, friendship, and insight of Dr. Thomas Stossel.

This work was supported by grants HL 27971, HL 19429, and RR 01902 from the National Institutes of Health, grant DCB 8517973 from the National Science Foundation; and grants from the Council for Tobacco Research and the Edwin S. Webster Foundation.

Received for publication 17 January 1986, and in revised form 28 May 1986.

### *References*

1. Allison, A. C., P. Davies, and S. De Petris. 1971. Role of contractile microfilaments in macrophage movement and endocytosis. *Nature New Biol.* 232:153–155.

2. Amato, P. A., E. R. Unanue, and D. L. Taylor. 1983. Distribution of actin in spreading macrophages: a comparative study on living and fixed cells. *J. Cell Biol.* 96:750–761.

3. Bennett, J. P., K. S. Zaner, and T. P. Stossel. 1984. Isolation and some properties of macrophage α-actinin: evidence that it is not an actin gelling protein. *Biochemistry.* 23:5081–5086.

4. Berlin, R. D., and J. M. Oliver. 1978. Analogous ultrastructure and surface properties during capping and phagocytosis in leukocytes. *J. Cell Biol.* 77:789–804.

5. Blikstad, I., F. Markey, L. Carlsson, T. Persson, and U. Lindberg. 1978. Selective assay of monomeric and filamentous actin in cell extracts using inhibition of deoxyribonuclease I. *Cell.* 15:935–943.

6. Bray, D., and C. Thomas. 1975. The actin content of fibroblasts. *Biochem. J.* 147:221–228.

7. Brotschi, E. A., J. H. Hartwig, and T. P. Stossel. 1978. The gelation of actin by actin-binding protein. *J. Biol. Chem.* 253:8988–8993.

8. Carlsson, L. E., I. Nystrom, F. Markey, and U. Lindberg. 1977. Actin polymerizability is influenced by profilin, a low molecular weight protein in non-muscle cells. *J. Mol. Biol.* 115:465–483.

9. Davies, W. A., and T. P. Stossel. 1977. Peripheral hyaline blebs (podosomes) of macrophages. *J. Cell Biol.* 75:941–955.

10. de Mey, J., M. Moeremans, G. Geuens, R. Nuydens, and M. de Brabander. 1981. High resolution light and electron microscopic localization of tubulin with the IGS (immuno gold staining) method. *Cell Biol. Int. Rep.* 5:889–899.

11. Deleted in press.

12. DiNubile, M. J., and F. S. Southwick. 1985. Effects of macrophage profilin on actin in the presence and absence of acumentin and gelsolin. *J. Biol. Chem.* 260:7402–7409.

13. Faulk, W. P., and G. M. Taylor. 1971. An immunocolloid method for the electron microscope. *Immunochemistry.* 8:1081–1083.

14. Fox, J. E. B. 1985. Identification of actin-binding protein as the protein linking the membrane skeleton to glycoproteins on platelet plasma membranes. *J. Biol. Chem.* 260:11970–11977.

15. Geuze, H. J., J. W. Slot, P. A. van der Ley, and R. C. T. Scheffer. 1981. Use of colloidal gold particles in double-labeling immunoelectron microscopy of ultrathin frozen tissue sections. *J. Cell Biol.* 89:653–665.

16. Gu, J., J. de Mey, M. Moeremans, and J. M. Polak. 1981. Sequential use of PAP and immunogold staining methods for the light microscopical double staining of tissue antigens. *Reg. Peptides.* 1:365–374.

17. Hancock, K., and V. C. W. Tsang. 1983. India ink staining of proteins on nitrocellulose paper. *Anal. Biochem.* 133:157–162.

18. Hanson, J., and J. Lowy. 1963. The structure of F-actin and of actin filament isolated from muscle. *J. Mol. Biol.* 6:46–60.

19. Hartwig, J. H., and T. P. Stossel. 1981. The structure of actin-binding protein molecules in solution and interacting with actin filaments. *J. Mol. Biol.* 145:563–581.

20. Hartwig, J. H., J. Tyler, and T. P. Stossel. 1980. Actin-binding protein promotes the bipolar and perpendicular branching of actin filaments. *J. Cell Biol.* 87:841–848.

21. Herman, I. M., and T. D. Pollard. 1979. Comparison of purified anti-actin and fluorescent-heavy meromyosin staining patterns in dividing cells. *J. Cell Biol.* 80:509–520.

22. Heuser, J. E., and M. W. Kirschner. 1980. Filament organization revealed in platinum replicas of freeze-dried cytoskeletons. *J. Cell Biol.* 86:212–234.

23. Laemmli, U. K. 1970. Cleavage of structural proteins during the assembly of the head of bacteriophage T4. *Nature (Lond.).* 227:680–685.

24. Lamarck, J. B. P. A. 1835. *Histoire naturelle des animaux sans vertebres.* J. B. Bailliere, Paris. 1:337–345.

25. Langanger, G., J. de May, M. Moeremans, G. Daneels, M. de Brabander, and J. Small. 1984. Ultrastructural localization of α-actinin and filamin in cultured cells with the immunogold staining (IGS) method. *J. Cell Biol.* 99:1324–1334.

26. Lewis, W. H. 1939. The role of a superficial plasmagel layer in changes of form, locomotion, and division of cells in tissue cultures. *Arch. Exp. Zellforsch.* 23:1–7.

27. Lowry, O. H., N. J. Rosebrough, A. L. Farr, and R. J. Randall. 1951. Protein measurements with the Folin phenol reagent. *J. Biol. Chem.* 193:265–275.

28. Margossian, S., and S. Lowey. 1978. Interaction of myosin subfragments with f-actin. *Biochemistry.* 17:5431–5439.

29. Myrvik, Q. N., E. S. Leake, and B. Fariss. 1961. Studies on pulmonary alveolar macrophages from the normal rabbit: a technique to procure them in a high state of purity. *J. Immunol.* 86:128–132.

30. Niederman, R., P. Amrein, and J. H. Hartwig. 1983. The three-dimensional structure of actin filaments and of an actin gel made with actin-binding protein. *J. Cell Biol.* 96:1400–1413.

31. Okita, L. R., D. Pidard, P. J. Newman, R. R. Montgomery, and T. J. Kunicki. 1985. On the association of glycoprotein Ib and actin-binding protein in human platelets. *J. Cell Biol.* 100:317–321.

32. Peterson, G. L. 1979. Review of the folin protein quantitation method of Lowry, Rosebrough, Farr, and Randall. *Anal. Biochem.* 100:201–220.

33. Schliwa, M., and J. van Blerkom. 1981. Structural interaction of cytoskeletal components. *J. Cell. Biol.* 90:222–235.

34. Schliwa, M., J. van Blerkom, and K. Porter. 1981. Stabilization of the cytoplasmic ground substance in detergent-opened cells and a structural and biochemical analysis of its composition. *Proc. Natl. Acad. Sci. USA.* 78:4329–4333.

35. Slot, J. W., and H. J. Geuze. 1981. Sizing of protein A-colloidal gold probes for immunoelectron microscopy. *J. Cell Biol.* 90:533–536.

36. Stendahl, O. I., J. H. Hartwig, E. A. Brotschi, and T. P. Stossel. 1980. Distribution of actin-binding protein and myosin in macrophages during spreading and phagocytosis. *J. Cell Biol.* 84:215–224.

37. Stossel, T. P., J. H. Hartwig, and H. L. Yin. 1981. Actin gelation and the structure and movement of cortical cytoplasm. *In Cytoskeletal Elements and Plasma Membrane Organization.* G. Poste and G. L. Nicolson, editors. Elsevier/North Holland, Amsterdam. 140–168.

38. Stossel, T. P., C. Chaponnier, R. M. Ezzell, J. H. Hartwig, P. A., Janmey, D. J. Kwiatkowski, S. E. Lind, D. B. Smith, F. S. Southwick, H. L. Yin, and K. S. Zaner. 1985. Nonmuscle actin-binding proteins. *Annu. Rev. Cell Biol.* 1:353–402.

39. Towbin, H., T. Staehelin, and J. Gordon. 1979. Electrophoretic transfer of proteins from polyacrylamide gels to nitrocellulose sheets: procedure and some applications. *Proc. Natl. Acad. Sci. USA.* 76:4350–4354.

40. Von Rosenhof, A. J. Roesel. 1792. *Insecten belustigungen.* Nurnberg: Kleeman (Neue Edition).

41. Yin, H. L., J. Albrecht, and A. Fattoum. 1981. Identification of gelsolin, a $Ca^{2+}$-dependent regulatory protein of actin gel-sol transformation: its intracellular distribution in a variety of cells and tissues. *J. Cell Biol.* 91:901–906.